Sleep Monitoring with Portable Wi-Fi

Name1 Surname[1,2]❂, Name2 Surname[2]❂, Name3 Surname[2,3]¤, Name4 Surname[2], Name5 Surname[2‡], Name6 Surname[2‡], Name7 Surname[1,2,3]*, with the Lorem Ipsum Consortium¶

1 Affiliation Dept/Program/Center, Institution Name, City, State, Country
2 Affiliation Dept/Program/Center, Institution Name, City, State, Country
3 Affiliation Dept/Program/Center, Institution Name, City, State, Country

❂These authors contributed equally to this work.
‡These authors also contributed equally to this work.
¤Current Address: Dept/Program/Center, Institution Name, City, State, Country
†Deceased
¶Membership list can be found in the Acknowledgments section.
* correspondingauthor@institute.edu

Abstract

WiFi human sensing is being challenged by researchers continuously e.g. Activity Classification, Localization and etc. However, we believed WiFi can do more. In this paper, we paired WiFi transmitting pattern to human sleep stage to create a mapping rule of those. we strengthened WiFi signal with 2 directional external antennae. After gathering WiFi variation from a router and sleep stage from a smartwatch, we applied machine learning to merge them. We used Long-short term memory (LSTM) to the framework since we know WiFi data tells more with its sequence. So, we are to map a sequence of sleeping stage to a sequence of WiFi snapshots instead of one-to-one like others which makes this called "Sleep monitoring". we tested with newly collected data sizing more than 100,000 frames of sequences. To evaluate the result, we compared annotated sleep stage with predicted sleep stage and summarized their distance error which finally resulted as that it is possible to classify 4 human sleep stages from WiFi.

Introduction

Wi-Fi is one of the most common network mediums nowadays. Pervasively, it is used for establishing a wireless network to connect to the internet. But, there are still many more functions Wi-Fi is good at. Wi-Fi can also be applied in fields beside connecting to the internet according to its stability being upgraded continuously. Decent Wi-Fi connectivity can extract more data other than the data to be transmitted like concentration, speed, obstacle between the transmission. Those can be composed to be many useful applications like Localization, Activity Classification and etc.

In order to achieve the applications like mentioned, There are many works tried to extract deep features from Wi-Fi. But, they are mostly working with very specific tools and Network Interface Card (NIC) connected to a laptop running Linux that is currently one of the ways allowing to obtain fine-grain Channel State Information (CSI), the descriptive data of the Wi-Fi propagating in that environment. Those limitations significantly decrease simplicity of implementation. It is hard for public demonstration and integration with many updated tools.

Actually, there are other existing ways for obtaining the CSI. One is from a ubiquitously used microprocessor, ESP32. which is still not much explored in Wi-Fi exploiting field. It is simple to implement and can be easily integrated with other tools in many platforms due to its massively produced external tools.

Human sleep stage monitoring is being observed for a whlie and recently applied on commercial products. As sleeping is significant to all persons and can lead to many serious deceases, people are more concerned on utilizing their sleepness with using devices those are able to inform them their sleep information e.g. smartwatches, smart mattress, smart rings and etc. But, those devices are considerably affect sleepness since it needs to contact with users' bodies.

So, this paper proposes a contactless sleep monitoring with Wi-Fi CSI from ESP32 where users can applied with easy-to-find microprocessor and monitor their sleep stage without contacting to their bodies. This allows sleep monitoring to be practical for other researchers and those who want to utilize their sleepness.

Background

Human sleep stage monitoring

Human sleep stage monitoring is widely used as stated above. There are many types of staging. But most common and what we chose are stages of 4 which are Wake, Light Sleep, Deep Sleep, REM (Rapid Eye Movement). Many tools can inform this information in time sequence and various at accuracy. We use .... as our ground truth as it is the most accurate among others (ref). The ..... can log stages with resolution of 30 seconds so, we consider a sequence of 30-second stage with a sequence of 30-second CSI data from Wi-Fi.

Wi-Fi

Wi-Fi is a well-known connectivity with no wire needed (wireless). It has been used as a medium for connecting to the internet for over 10 years. However, the Wi-Fi is the name covering IEEE 802.11 n/g/ac protocols. It delivers data through 2.4/5GHz frequency with multiple channels. The bandwidth in each channel is 22MHz. the data are to be transmitted parallelly with multiplexing technique named orthogonal frequency division multiplexing (OFDM). Each carrier may propagate to a receiver with encountering many obstacles. The effect of that situation is the Doppler Effect. So, Channel State Information (CSI) is represented as physical layer indicator that can be used to investigate how each channel propagate to the receiver or back to the transmitter.

If a sender sends data to a receiver through Wi-Fi, the data will be almostly not transmitted without any loss.

CSI data

As mentioned in Wi-Fi that data propagating to the receiver while touching surrounding environment, the CSI is a variation of the data. The CSI can be found at both sender and receiver since receiver may transmit data back. Let the sender use the modulation method of 16-quadrature amplitude modulation (16-QAM) which one carrier can carry 4 bits. When the sender needs to send a '1111', the modulation returns $x = 1 + 1i$. Then, transmit to the receiver. At the receiver, let the obtained data is $y = 0.8 + 0.9i$. So, the CSI can be computed by the variation $h = y/x = 0.2 + 3.4i$.

Human body is literally water which reflect radio wave like Wi-Fi. [6], [7] and [8] have proven that human body can affect the CSI.

ESP32

ESP32 is a very popular single-board computer (SBC). With its affordable price and many available additional tools, ESP32 is commonly used in Internet of Things field. Moreover, it can be applied in research field. Quantitative CSI can be obtained from Wi-Fi in ESP32 according to [26]. The number of available subcarriers in ESP32 is 64.

According to the detail about Wi-Fi mentioned in Wi-Fi, the Wi-Fi in ESP32 has some limitation. It supports only 2.4GHz frequency and can be set only one channel over a connection. The bandwidth of each channel is 22MHz. The CSI can be both obtain from Access point (AP) and Station (STA) as shown in Fig 1. In this paper, we consider to mainly use CSI at the AP. The frequency of each channel is as 802.11 standard.
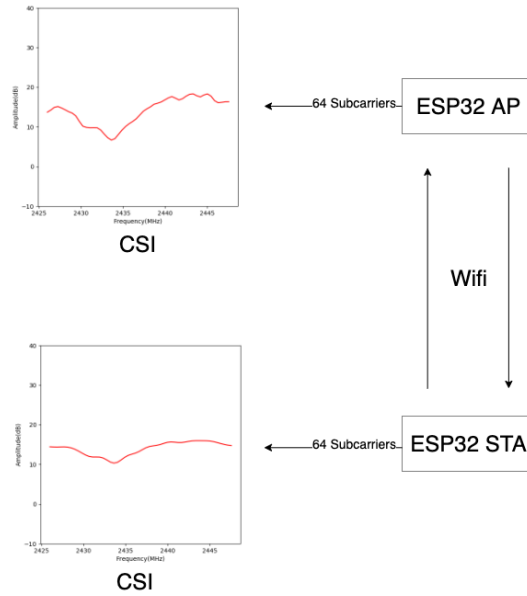

Fig 1. CSI from ESP32s with channel 6.

Materials and methods

Concept

Other famous proposed works like [6] [7] and [25] focus on line-of-sight (LOS) in between AP and STA while our work uses 2 directional Wi-Fi antennae and focus on reflection from human body as shown in Fig 2 on the left.

The CSI is not only affected by human body but mainly by overall environment. This means that 2 identical human poses can result obviously different CSIs if the environment around are not exactly the same as shown in Fig 2.

So, the definite detection of human standing still in every environment is nearly impossible since the CSI of that situation may be found exactly matched to a CSI of the environment that a big bottle of water placed in front of ESP32. In short, if it does not move, we do not know if it is a human.

Meanwhile, the moving pose is totally different because we focus on its change instead. The example of mapping CSI's change to Activity Classification can be found
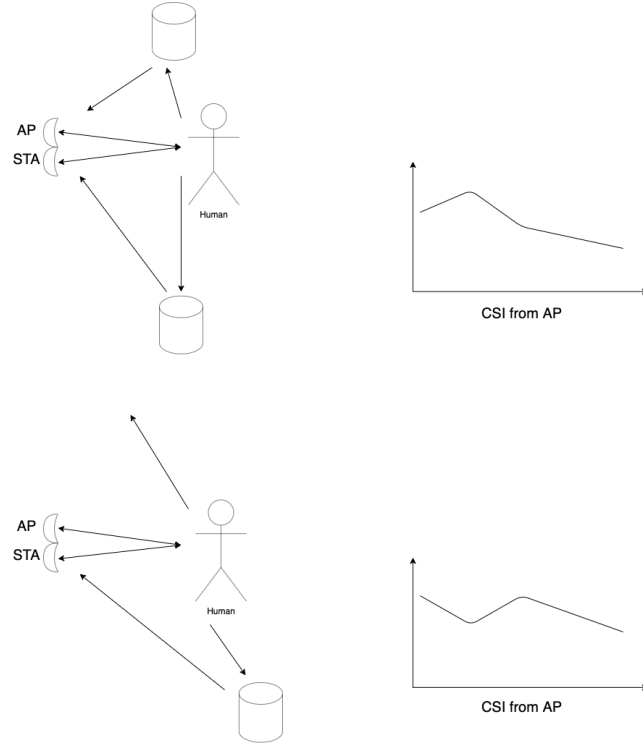
Fig 2. 2 different CSIs resulted from corresponding human poses.

in [8] and [27]. Our work does likewise but focusing on Sleep stage monitoring instead of Activity Classification.

In different environment, the CSIs are different. But, the corresponding changing of sleep stage may affect to the same changing pattern of CSI. This hypothesis is investigated in the upcoming parts.

All steps of training method is shown in Fig 3.

Pre-processing

CSI Resampling

As mentioned in ESP32, there are 64 subcarriers in CSI data from ESP32 but there are only 52 those are usable while the rest are null. So, we can construst a tensor of 1×52 to represent each CSI. We are to map CSI from the ESP32 to human sleep stage from .... The sampling rate of the ..... can log sleep stage once 30 seconds since its limitation. So, we have one sleep stage annotations for 30 seconds. For the ESP32, the sampling rate is originally unpredictable and not constant but it is running around 120Hz. So, we do a process called "Resampling" to obtain CSI at rate 30Hz in order to maintain the dimension of each sequence.

An example of CSI Resampling is shown in Fig 4. The top graph shows that the the original CSI is logged unstably. The bottom one is to pick a timestamp at rate 30Hz and calculated each with 2 data at the closet timestamps from the original with a simple mathematical weight equation as in Eq. 1 in order to predict CSI at timestamp corresponding to each human pose annotation.
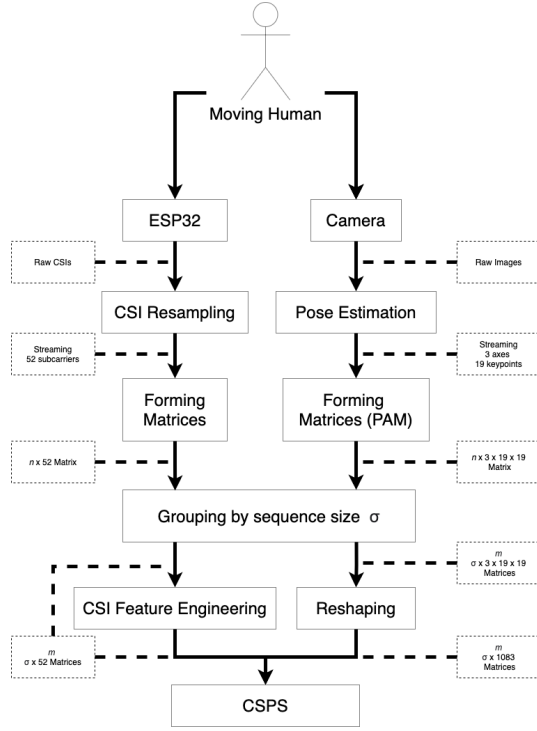
Fig 3. All steps of training method.

$$CSI_{now} = CSI_{before}$$
$$+ \left(\frac{ts_{now} - ts_{before}}{ts_{after} - ts_{before}} \times (CSI_{after} - CSI_{before}) \right), \tag{1}$$

where ts_{now}, ts_{before}, ts_{after} are desired timestamp, timestamp at the closest CSI before   107
the desired timestamp and timestamp at the closest CSI after the desired timestamp   108
respectively. And, CSI_{now}, CSI_{before}, CSI_{after} are CSI at the desired timestamp, CSI   109
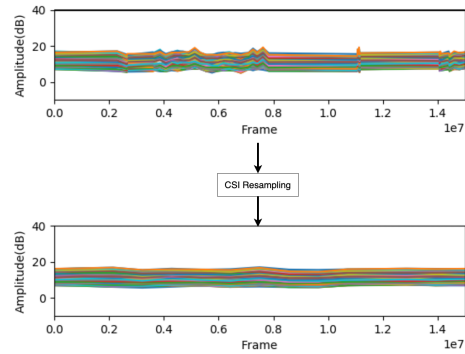before the desired timestamp and CSI after the desired timestamp respectively.   110

Fig 4. An example of CSI resampling.

Thus, we are able to map each CSI sequence of 30 seconds to one sleep stage   111
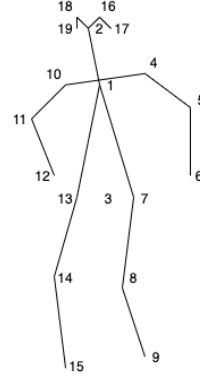annotation at the corresponding timestamp.   112

Fig 5. 19 keypoints of human pose.

We use Github-Lw3d[1] to estimate 3D human pose from videos as stated above. the ^{114}
estimation gives us a 19×3 matrix for each image. The 19×3 matrix are used as an ^{115}
annotation where 19 is for keypoints in human body and 3 is for 3 axes coordination as ^{116}
shown in Fig 5. But, the annotation can still possess too much independency. Some ^{117}
alignment of keypoints may lead to some impossible pose e.g. hip keypoint found very ^{118}
far from neck keypoint or head keypoint attached to hip keypoint. We assume those ^{119}
poses are not possible for normal human pose. To preserve those constraints, we form a ^{120}
pose adjacent matrix (PAM) from an original 19×3 matrix. the PAM is applied for all ^{121}
x, y and z axes. Each are to form their 19×19 matrix by the following equations. ^{122}

$$x'_{i,j} = \begin{cases} x_i - x_j & i \neq j \\ x_i & i = j \end{cases} \tag{2}$$

, ^{123}

$$y'_{i,j} = \begin{cases} y_i - y_j & i \neq j \\ y_i & i = j \end{cases} \tag{3}$$

and ^{124}

$$z'_{i,j} = \begin{cases} z_i - x_j & i \neq j \\ z_i & i = j \end{cases} \tag{4}$$

. ^{125}

The PAM is finally a $3 \times 19 \times 19$ matrix created from 3 matrices of x', y' and z' ^{126}
stacked. Apparently, one PAM represents one human pose. ^{127}

Conclusively, we are making a model by mapping a sequence of 1×52 matrix from ^{128}
CSI to each sequence of $19 \times 3 \times 3$ PAM from moving human pose annotation with the ^{129}
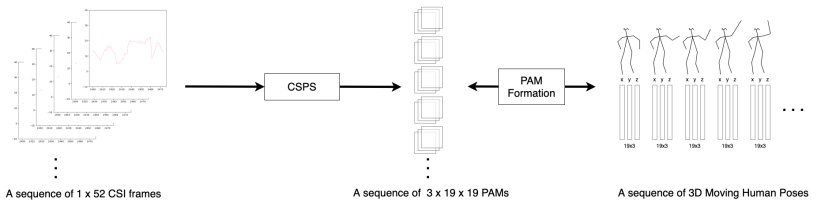corresponding timestamp as shown in Fig 6. ^{130}

Fig 6. A mapping rule from CSI frames to 3D human poses.

[1]https://github.com/Daniil-Osokin/lightweight-human-pose-estimation-3d-demo.pytorch

Processing

Mapping CSI and PAM

Let D be a set of synchronized pose and CSI data package. Each pair has corresponding timestamp.

$$D = (C_t, P_t), t \in [1, n], \tag{5}$$

where n is a number of pairs, C is for CSI data from ESP32, P is for PAM annotation as the ground truth and t is the timestamp index when those 2 were collected.

Grouping By Sequence Size

Let σ be an adjustable window size. σ size of D are fed to the model solely. So, $\sigma \leq n$. And, Let m be the number of feeding iteration, $m = \lfloor \frac{n}{\sigma} \rfloor$.

The training model swallow m training data as an input, where each is a sequencial set of (C_t, P_t) at a corresponding timestamp with size σ. Let Γ be a representation of each sequencial set.

$$\Gamma = (C_u, P_u), u \in [1, \sigma], \tag{6}$$

where u is the timestamp index when those 2 were collected. Apparently, the size of Γ is m.

As the Γ is a sequencial set with size σ, we assume that Long-short term memory (LSTM) [28] is suitable for this type of data.

CSI Feature Engineering

As mentioned in Concept, CSI (C) value implies environment where signal propagating. So, we need to ignore it and focus only on its change in order to universalize the circumstance. It means CSI variousity makes the model not to be applicable in every environment. To solve it, we simply sequentially substract C_u in each Γ backward to preserve only how CSI changes over each sequence by the following equation,

$$C_u = \begin{cases} \text{all } 0 & u = 1 \\ C_u - C_{u-1} & u > 1 \end{cases}, C_u \in \Gamma. \tag{7}$$

Forming Network Layer

CSI Sequence to Pose Sequence (CSPS) The summation of layers is shown in Table 1. It is designed to shape a CSI Sequence ($\sigma \times 52$ tensor) to a predicted sequence of pose ($\sigma \times 3 \times 19 \times 19$ tensor).

Table 1. Layers in CSPS.

Layer (type)	Output Shape	Param #
Bidirectional LSTM	(None, 200)	122400
RepeatVector	(None, σ, 200)	0
Bidirectional LSTM	(None, σ, 200)	240800
TimeDistributed over Dense	(None, σ, 1083)	217683

We first use Bidirectional LSTM as an encoder layer with the input size of $(\sigma, 52)$ to satisfy dimension of sequential C_u in Γ. Then, the repeat vector is added with time σ to

make the model treat with correct time-step. Afterward, we place a decoder layer with another Bidirectional LSTM.

Next, we dense the decoder to be 1083 where can be reshaped into $3 \times 19 \times 19$ later.

Lastly, the TimeDistributed layer is used in order to make the model treat the output for each time-step individually.

Results

Data Collection

We recruited 10 volunteers to act common movements in front of the devices (a camera and WiFi anntennae) in 3 different environments. The example of the data collection are shown in Fig. 7 and Fig. 8 where the top-left is the annotated Pose Estimation, the top-right is a raw video, the vertical center is a raw WiFi CSI and the bottom is a resampled WiFi CSI.

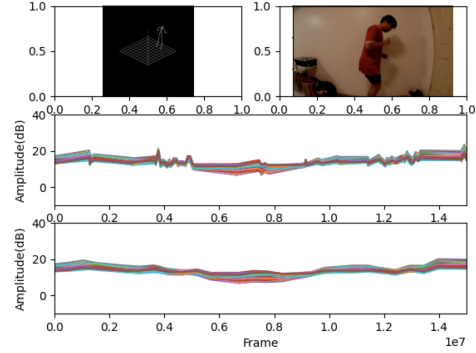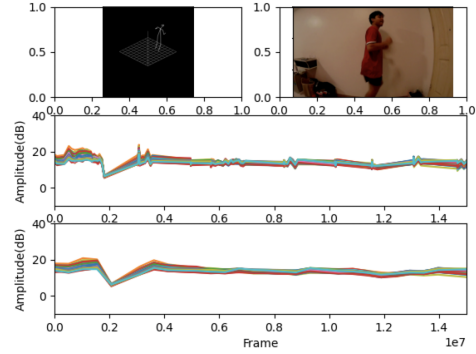**Fig 7.** An example of data collection.

Fig 8. An example of data collection.

The whole data collected is an hour of videos and WiFi CSI which worths 180,000 frames for 30 fps rate. The ratio of dataset for training and testing is 80/20.

Error Metric

Percentage of Correct Keypoint (PCK) is widely used to evaluate the performance of human pose estimation according to [6].

$$PCK_i@a = \frac{1}{N} \sum_{i=1}^{N} I\left(\frac{\parallel pd_i - gt_i \parallel_2^2}{\sqrt{rh^2 + lh^2}} \le a\right), \tag{8}$$

where $I(\cdot)$ is a binary indicator that outputs 1 while true and 0 while false, N is the number of frames and i is the index of keypoints that $i \in 1, 2, ..., 19$. The rh and lh are for the positions of the right shoulder and the left hip from the ground truth, respectively. So, the $\sqrt{rh^2 + lh^2}$ is considered as the length of the upper limb from the ground truth, which is used to normalize the prediction error length $\parallel pd_i - gt_i \parallel_2^2$, and pd_i and gt_i are coordinates of prediction and ground-truth at the keypoint i respectively.

Experimental Result

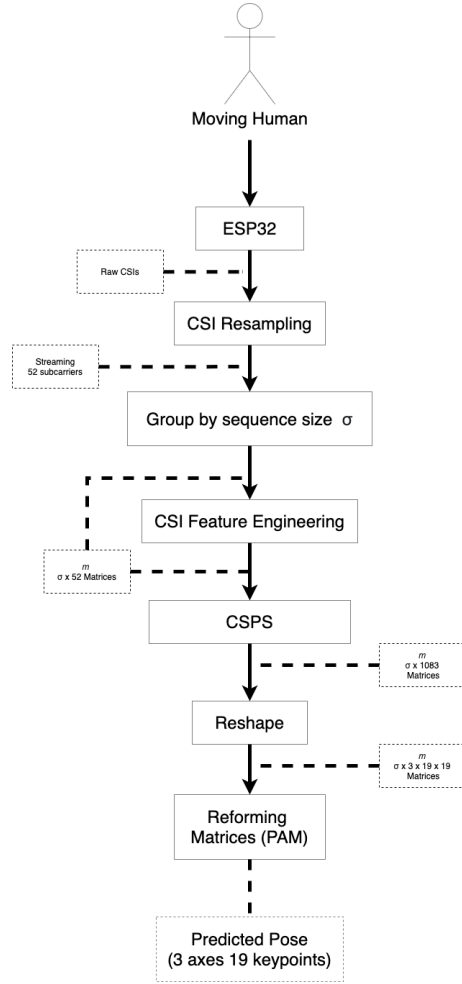All steps of testing method is shown in Fig 9.

Fig 9. All steps of testing method.

An evaluation is achieved by the algorithm written in Python 3.8. The code is available on Github[1]. An environment under the evaluation is MacBook Pro 2016, 2.6 GHz i7 processor, 16 GB of RAM.

---

[1]https://github.com/rtmtree/CSPS

The visual examples are shown in 10 and 11 where the top-left is the predicted pose, the top-right is the annotated pose and bottom is the resampled WiFi CSI that the prediction took as an input. Note that the predicted and the annotated pose are actually moving in range of σ.
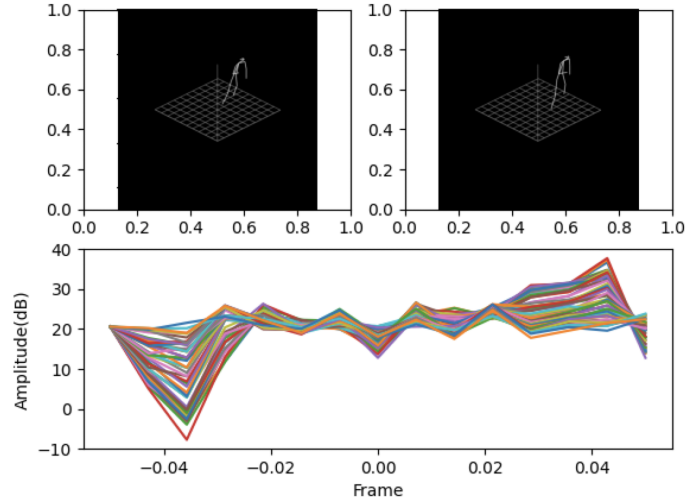

Fig 10. An example of comparison between predicted pose and annotated pose when $\sigma = 15$.

As parameters stated in the previous sections, we demostrated the prediction by the followings.

Table 2, Table 3, Table 4 and Table 5 show the estimation performance of 19 body keypoints in PCK when $\sigma = 15$, $\sigma = 20$, $\sigma = 30$ and $\sigma = 40$ respectively.

Discussion

WiFi Antennae and Camera Installation

The Installation of WiFi antennae and camera can affect tremendously in data. We used a hanger and a camera stand to lock the fixed installation in both training and testing process as shown in Fig 12. 2 antennae are connecting to ESP32s and to the PC afterward.

CSI Extraction Method

There are many soluions for extracting WiFi CSI from the ESP as mentioned in ESP32. This paper picked the solution from ESP32-CSI-Tool[1] since it is considerably well-written and simple to organize. To change the method of extracting WiFi CSI would affect the result significantly.

Multiple Person Pose Estimation

The model does the mapping rule from WiFi CSI with a specific dimension to human pose matrix. So, it is able to only detect single person pose in a range. The annotations
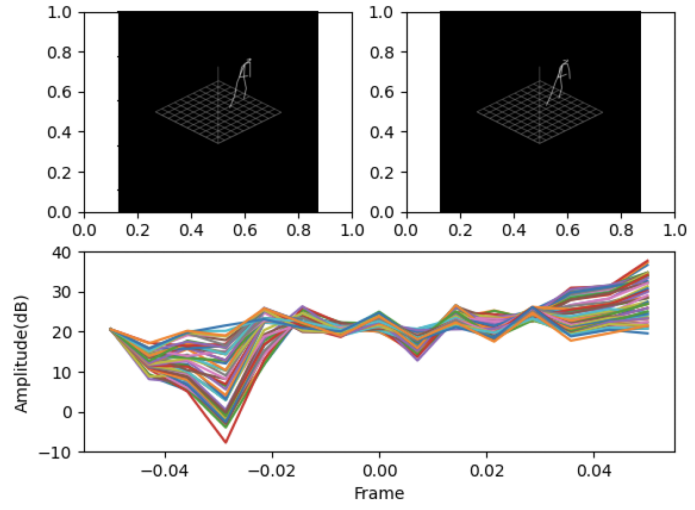
---

[1]https://github.com/StevenMHernandez/ESP32-CSI-Tool

Fig 11. An example of comparison between predicted pose and annotated pose when $\sigma = 15$.

Fig 12. WiFi Antennae and Camera Setup.

Table 2. Table of PCK when $\sigma = 15$.

Order	Keypoint	PCK@5	PCK@10	PCK@20	PCK@30	PCK@40	PCK@50
1	Neck	0.7553	0.8993	0.9443	0.9590	0.9717	0.9810
2	Nose	0.0383	0.4885	0.9038	0.9498	0.9649	0.9724
3	Hip (Invisible)	0.7626	0.9033	0.9437	0.9583	0.9688	0.9796
4	L. Shoulder	0.6502	0.8436	0.9426	0.9665	0.9766	0.9828
5	L. Elbow	0.6055	0.7786	0.9001	0.9482	0.9681	0.9772
6	L. Wrist	0.3149	0.5845	0.8135	0.9013	0.9415	0.9625
7	L. Hip	0.6866	0.8678	0.9485	0.9653	0.9765	0.9862
8	L. Knee	0.5571	0.7794	0.9194	0.9587	0.9747	0.9837
9	L. Ankle	0.4132	0.6572	0.8617	0.9292	0.9583	0.9740
10	R. Shoulder	0.6419	0.8407	0.9364	0.9527	0.9618	0.9709
11	R. Elbow	0.5966	0.7596	0.8854	0.9321	0.9532	0.9632
12	R. Wrist	0.3031	0.5936	0.8204	0.9132	0.9386	0.9496
13	R. Hip	0.6895	0.8690	0.9404	0.9547	0.9663	0.9778
14	R. Knee	0.5626	0.7750	0.9169	0.9493	0.9631	0.9753
15	R. Ankle	0.4370	0.6611	0.8627	0.9301	0.9552	0.9711
16	L. Eye	0.0279	0.4281	0.8955	0.9493	0.9638	0.9740
17	L. Ear	0.0677	0.6447	0.9250	0.9571	0.9709	0.9830
18	R. Eye	0.0204	0.2476	0.8729	0.9476	0.9617	0.9706
19	R. Ear	0.0326	0.5010	0.9182	0.9527	0.9638	0.9729
Avg		0.4296	0.6907	0.9027	0.9461	0.9631	0.9741

Table 3. Table of PCK when $\sigma = 20$.

Order	Keypoint	PCK@5	PCK@10	PCK@20	PCK@30	PCK@40	PCK@50
1	Neck	0.7698	0.9026	0.9511	0.9658	0.9748	0.9816
2	Nose	0.6612	0.8463	0.9452	0.9625	0.9710	0.9771
3	Hip (Invisible)	0.7601	0.9025	0.9522	0.9671	0.9750	0.9815
4	L. Shoulder	0.6680	0.8563	0.9483	0.9717	0.9810	0.9864
5	L. Elbow	0.6056	0.7845	0.9051	0.9571	0.9753	0.9827
6	L. Wrist	0.3196	0.5872	0.8178	0.9027	0.9400	0.9614
7	L. Hip	0.6827	0.8711	0.9508	0.9700	0.9805	0.9873
8	L. Knee	0.5637	0.7773	0.9169	0.9584	0.9767	0.9844
9	L. Ankle	0.4373	0.6639	0.8598	0.9269	0.9571	0.9740
10	R. Shoulder	0.6589	0.8506	0.9444	0.9618	0.9705	0.9757
11	R. Elbow	0.5979	0.7650	0.8904	0.9394	0.9636	0.9725
12	R. Wrist	0.2985	0.5901	0.8169	0.9148	0.9465	0.9593
13	R. Hip	0.6917	0.8765	0.9501	0.9637	0.9728	0.9800
14	R. Knee	0.5676	0.7853	0.9259	0.9561	0.9682	0.9774
15	R. Ankle	0.4532	0.6723	0.8734	0.9385	0.9600	0.9730
16	L. Eye	0.6721	0.8515	0.9455	0.9632	0.9723	0.9785
17	L. Ear	0.7239	0.8810	0.9482	0.9660	0.9762	0.9843
18	R. Eye	0.6658	0.8477	0.9459	0.9626	0.9706	0.9764
19	R. Ear	0.7091	0.8810	0.9492	0.9631	0.9715	0.9775
Avg		0.6056	0.7996	0.9177	0.9532	0.9686	0.9774

originally result all human poses from the videos but we decided to crop it to be only 209
one person in order to increase the precision. If we do training with multiple person 210
pose data instead, we believe the result will be well but the more huge data collection is 211

Table 4. Table of PCK when $\sigma = 30$.

Order	Keypoint	PCK@5	PCK@10	PCK@20	PCK@30	PCK@40	PCK@50
1	Neck	0.7580	0.8866	0.9373	0.9547	0.9654	0.9748
2	Nose	0.6631	0.8315	0.9315	0.9512	0.9620	0.9688
3	Hip (Invisible)	0.7507	0.8873	0.9390	0.9561	0.9659	0.9759
4	L. Shoulder	0.6680	0.8418	0.9300	0.9564	0.9703	0.9785
5	L. Elbow	0.6143	0.7760	0.8943	0.9426	0.9644	0.9740
6	L. Wrist	0.3116	0.5755	0.8023	0.8888	0.9316	0.9541
7	L. Hip	0.6828	0.8597	0.9366	0.9590	0.9694	0.9806
8	L. Knee	0.5584	0.7719	0.9096	0.9492	0.9669	0.9778
9	L. Ankle	0.4332	0.6620	0.8575	0.9215	0.9498	0.9665
10	R. Shoulder	0.6719	0.8453	0.9322	0.9495	0.9613	0.9696
11	R. Elbow	0.6255	0.7772	0.8859	0.9331	0.9548	0.9653
12	R. Wrist	0.3134	0.6091	0.8155	0.9038	0.9336	0.9477
13	R. Hip	0.6974	0.8637	0.9361	0.9536	0.9673	0.9770
14	R. Knee	0.5828	0.7854	0.9127	0.9455	0.9617	0.9730
15	R. Ankle	0.4678	0.6847	0.8693	0.9303	0.9523	0.9671
16	L. Eye	0.6712	0.8364	0.9316	0.9518	0.9629	0.9704
17	L. Ear	0.7145	0.8664	0.9337	0.9544	0.9660	0.9767
18	R. Eye	0.6648	0.8322	0.9322	0.9508	0.9612	0.9685
19	R. Ear	0.7068	0.8645	0.9350	0.9522	0.9622	0.9709
Avg		0.6082	0.7925	0.9064	0.9423	0.9594	0.9704

Table 5. Table of PCK when $\sigma = 40$.

Order	Keypoint	PCK@5	PCK@10	PCK@20	PCK@30	PCK@40	PCK@50
1	Neck	0.7480	0.8822	0.9339	0.9519	0.9658	0.9746
2	Nose	0.6546	0.8270	0.9273	0.9484	0.9614	0.9707
3	Hip (Invisible)	0.7435	0.8832	0.9361	0.9542	0.9675	0.9780
4	L. Shoulder	0.6703	0.8406	0.9263	0.9529	0.9683	0.9781
5	L. Elbow	0.6156	0.7802	0.8968	0.9398	0.9618	0.9727
6	L. Wrist	0.3259	0.5890	0.8076	0.8939	0.9330	0.9551
7	L. Hip	0.6649	0.8491	0.9339	0.9556	0.9684	0.9805
8	L. Knee	0.5393	0.7585	0.9044	0.9471	0.9663	0.9765
9	L. Ankle	0.4188	0.6476	0.8437	0.9162	0.9485	0.9664
10	R. Shoulder	0.6654	0.8353	0.9264	0.9473	0.9605	0.9703
11	R. Elbow	0.6245	0.7786	0.8791	0.9272	0.9525	0.9656
12	R. Wrist	0.3115	0.5966	0.8159	0.9057	0.9340	0.9481
13	R. Hip	0.6894	0.8598	0.9328	0.9525	0.9683	0.9785
14	R. Knee	0.5753	0.7826	0.9090	0.9448	0.9621	0.9737
15	R. Ankle	0.4619	0.6786	0.8663	0.9281	0.9521	0.9668
16	L. Eye	0.6629	0.8317	0.9274	0.9493	0.9630	0.9723
17	L. Ear	0.7088	0.8610	0.9302	0.9521	0.9678	0.9767
18	R. Eye	0.6579	0.8285	0.9269	0.9483	0.9608	0.9701
19	R. Ear	0.6950	0.8608	0.9312	0.9491	0.9629	0.9715
Avg		0.6018	0.7880	0.9029	0.9402	0.9592	0.9709

also needed.

Human speed of moving to σ

As the Table 2, Table 3, Table 4 and Table 5 show the difference of quality by different value of σ, the fine-tuning says that $\sigma = 15$ result the best. This implies length of 15 frames can represent a specific pattern of move best for the used dataset. So, the volunteer who recorded movement in the datasent perform a move slower, σ should be extended to cover the proper time peroid of the movement pattern.

Conclusion

Currently, there are many issues on security occuring in all ranges of human especially in elderlies and those who are not capable to live solely. To solve those, issues on privacy usually comes instead e.g. recording videos for preventing accident in a house, monitoring of people in a room. Many people do not feel very comfortable on these. So, we seek a solution where we can monitor those activity without a camera needed.

After having a research, we discoverd that a variation in WiFi called WiFi CSI can tell whether the area is having an activity or moving objects. Moreoever, [8], [27] and many other works had been done very well on detecting even what kind of activities is happening in the area. We do not believe that this is the limitation of WiFi CSI. In order to solve the above problem and prove if WiFi CSI is precise enough, we tried to overcome this by extracting a deeper information like Pose Estimation from it.

We controlled environments and enhanced WiFi Antennae stability as much as possible then mapped it to the Pose annotated by an existing Image to Pose Model. The result was very poor since the WiFi CSI is very vague. It penetrates through most of the things. We learned from [20] that WiFi CSI value does not matter than its change. The works used Long-short term memory (LSTM), a neural network where focusing on sequence of the data, and obtained a very good result.

We applied the idea of LSTM on our work which made it not Pose Estimation but Moving Pose Estimation instead and obtained a lot better result. Then, we adjusted the model to be suite to our type of data and did fine-tuning for the frame size to be fit the most for normal human speed of moving. So, This paper proposed a model of mapping rule that can takes a sequence of WiFi circumstance as an input and return an according sequence of human pose as an output. The work can help people to monitor activity of elderlies and people who are in need of caring. Moreover as a camera is not needed, we can reduce an issue on privacy infringement and also cure the data size normal camera conducted as WiFi CSI is carrying much lower data size. The result of various fine-tuned environments and parammeters is acceptable and shown in Experimental Result.

Acknowledgments

References

1. Conant GC, Wolfe KH. Turning a hobby into a job: how duplicated genes find new functions. Nat Rev Genet. 2008 Dec;9(12):938–950.

2. Ohno S. Evolution by gene duplication. London: George Alien & Unwin Ltd. Berlin, Heidelberg and New York: Springer-Verlag.; 1970.

3. Magwire MM, Bayer F, Webster CL, Cao C, Jiggins FM. Successive increases in the resistance of Drosophila to viral infection through a transposon insertion followed by a Duplication. PLoS Genet. 2011 Oct;7(10):e1002337.

4. Osokin D. Real-time 2D Multi-Person Pose Estimation on CPU: Lightweight OpenPose. arXiv:1811.12004 [cs.CV]. 2018 Nov;18.

5. Mehta D, Sotnychenko O, Mueller F, Xu W, Sridhar S, Pons-Moll G, Theobalt C. Single-Shot Multi-Person 3D Pose Estimation From Monocular RGB. arXiv:1712.03453 [cs.CV]. 2018 Aug;28.

6. Wang F, Panev S, Ziyi D, Han J, Huang D. Can WiFi Estimate Person Pose?. arXiv:1904.00277 [cs.CV]. 2019 Apr;2.

7. Liu J, Liu H, Chen Y, Wang Y, Wang C. Wireless Sensing for Human Activity: A Survey. IEEE COMMUNICATIONS SURVEYS & TUTORIALS, VOL. 22, NO. 3, THIRD QUARTER 2020.

8. Chowdhury TZ, Leung C, Miao CY. WiHACS: Leveraging WiFi for Human Activity Classification using OFDM Subcarriers' correlation. IEEE, GlobalSIP 2017.

9. Guo L, Wang L, Liu J, Zhou W, Lu B. HuAc: Human Activity Recognition Using Crowdsourced WiFi Signals and Skeleton Data. Wireless Communications and Mobile Computing Volume 2018, Article ID 6163475.

10. Wang F, Feng J, Zhao Y, Xiaobin Zhang, Zhang S. Joint Activity Recognition and Indoor Localization with WiFi Fingerprints. arXiv:1904.04964 [cs.CV]. 2019 Jul;18.

11. Al-qaness MAA, Li F, Ma X, Zhang Y, Liu G. Device-Free Indoor Activity Recognition System. Appl. Sci. 2016, 6, 329; doi:10.3390.

12. Wang W, Liu AX, Shahzad M, Ling K, Lu S. Device-free Human Activity Recognition Using Commercial WiFi Devices. IEEE Journal on Selected Areas in Communications. DOI 10.1109/JSAC.2017.2679658.

13. Zhao T, Li F, Tian P. A Deep-Learning Method for Device Activity Detection in mMTC Under Imperfect CSI Based on Variational-Autoencoder. IEEE TRANSACTIONS ON VEHICULAR TECHNOLOGY, VOL. 69, NO. 7, JULY 2020.

14. Liu J, Teng G, Hong F. Human Activity Sensing with Wireless Signals: A Survey. Sensors 2020, 20, 1210; doi:10.3390/s20041210.

15. Yousefi S, Narui H, Dayal S, Ermon S, Valaee S. A Survey on Behaviour Recognition Using WiFi Channel State Information. arXiv:1708.07129 [cs.AI]. 2017 Aug;23.

16. Chen Z, Zhang L, Jiang C, Cao Z, Cui W. WiFi CSI Based Passive Human Activity Recognition Using Attention Based BLSTM. IEEE TRANSACTIONS ON MOBILE COMPUTING, VOL. 18, NO. 11, 2019 Nov.

17. Li B, Cui W, Wang W, Zhang L, Chen Z, Wu M. Two-Stream Convolution Augmented Transformer for Human Activity Recognition. Association for the Advancement of Artificial Intelligence, 2021.

18. Luo Y, Ren J, Wang Z, Sun W, Pan J, Liu J, Pan J, Lin L. LSTM Pose Machines. arXiv:1712.06316 [cs.CV].

19. Lee K, Lee I, Lee S. Propagating LSTM: 3D Pose Estimation based on Joint Interdependency. Computer Vision – ECCV 2018. ECCV 2018. Lecture Notes in Computer Science, vol 11211. Springer, Cham.

20. Du X, Vasudevan R, Johnson-Roberson M. Bio-LSTM: A Biomechanically Inspired Recurrent Neural Network for 3D Pedestrian Pose and Gait Prediction. arXiv:1809.03705 [cs.RO]. 2019 Sep;13.

21. Hossain MRI, Little JJ. Exploiting temporal information for 3D human pose estimation. arXiv:1711.08585 [cs.CV]. 2018 Sep;12.

22. Pavllo D, Feichtenhofer C, Grangier D, Auli M. 3D human pose estimation in video with temporal convolutions and semi-supervised training. arXiv:1811.11742 [cs.CV]. 2019 Mar;29.

23. Chen T, Fang C, Shen X, Zhu Y, Chen Z, Luo J. Anatomy-aware 3D Human Pose Estimation with Bone-based Pose Decomposition. arXiv:2002.10322 [cs.CV]. 2021 Jan;26.

24. Ruiz AH, Porzi L, Bulo SR, Moreno-Noguer F. 3D CNNs on Distance Matrices for Human Action Recognition. MM '17, Mountain View, CA, USA. 2017 Oct;23–27.

25. Hernandez SM, Bulut E. Lightweight and Standalone IoT based WiFi Sensing for Active Repositioning and Mobility. IEEE 21st International Symposium on "A World of Wireless, Mobile and Multimedia Networks" (WoWMoM), 2020.

26. Atif M, Muralidharan S, Ko H, Yoo B. Wi-ESP—A tool for CSI-based Device-Free Wi-Fi Sensing (DFWS). Journal of Computational Design and Engineering, 2020, 7(5), 644–656.

27. Zou H, Zhou Y, Yang J, Jiang H, Xie L, Spanos CJ. DeepSense: Device-free Human Activity Recognition via Autoencoder Long-term Recurrent Convolutional Network. 2018 IEEE International Conference on Communications (ICC), Kansas City, MO, USA, 2018, pp. 1-6, doi: 10.1109/ICC.2018.8422895.

28. Hochreiter S, Schmidhuber J. LONG SHORT-TERM MEMORY. Neural Computation 9(8):1735-1780, 1997.